# COMPENSATED INVERSE PID CONTROLLER FOR ACTIVE VIBRATION CONTROL WITH PIEZOELECTRIC PATCHES: MODELING, SIMULATION AND IMPLEMENTATION

ASAN GANI, M.J.E SALAMI AND MD. RAISUDDIN KHAN

*Mechatronics Department, Faculty of Engineering, International Islamic University Malaysia*

*Jalan Gombak, 53100, Kuala Lumpur, MALAYSIA*

*E-mail: asan@iiu.edu.my*

***Abstract:*** Active vibration control of the first three modes of a vibrating cantilever beam using collocated piezoelectric sensor and actuator is examined in this paper. To achieve this, a model based on Euler-Bernoulli beam equation is adopted and extended to the case of three bonded piezoelectric patches that act as sensor, actuator and exciter respectively. A compensated inverse PID controller has been designed and developed to damp first three modes of vibration. Controllers have been designed for each mode and these are later combined in parallel to damp any of the three modes. Individual controller gives better reduction in sensor output for the second and third modes while the combined controller performs better for the first mode. Simulation studies are carried out using MATLAB. These results are compared and verified experimentally and the real-time implementation is carried out with xPC-target toolbox in MATLAB.

***Keywords:*** *Active control, Vibration suppression, Piezoelectric sensor/actuator, compensated inverse PID.*

## 1. INTRODUCTION

Advances in smart materials have shown many interesting applications of them for passive and active structural damping. Passive damping treatment has fixed frequency range and adds significant weight to the structures. To overcome these drawbacks piezoelectric materials have been advocated for use in order to have control over a wide range of frequencies without adding much weight to the structure. Research in piezoelectric materials is rapidly gaining attention and it is envisaged that such technology will widen the scope and enhance the quality of products in many manufacturing industries.

Vibration control using piezoelectric materials can be accomplished either passively with shunt circuit [1-3] or actively. In passive control, piezoelectric materials are used to damp the vibration via energy dissipation. In a vibrating structure, a shunt network can be configured to accomplish vibration control by modifying the dynamics of the electrical system [4,5]. This system is analogous to mass-spring dashpot system which acts as a vibration absorber. A properly tuned shunt circuit can add significant damping to a structure. In active vibration control (AVC), external power is applied to piezoelectric material to produce force in the direction opposite to that

produced by vibrating structure. The opposite forces would cancel each other and thus reduce system vibration. Increasing number of work has been done on active vibration control using piezoelectric materials. Different control algorithms have been developed and these can be classified under feedback and feedforward AVC. Some of the research work in AVC can be found in [6 – 18]. Baz and Poh [6] have used a modified independent modal space control with a piezoelectric and three displacement sensors to perform AVC on a beam. Hollkamp and Starchville [7] have employed six pairs of piezoelectric sensor/actuator to design self-tuning vibration absorber. In [9], Brennan, Elliott and Pinnington have used three different control strategies and of which one of them is to maximize power absorbing strategy. Morgan and Wang [18] used a combination of passive and active control strategies to reject variable frequency narrow band disturbance. In this paper, a rather simple configuration with only one pair of sensor actuator is used to control first three vibration modes. A compensated inverse PID controller has been designed to reduce multiple vibration modes of structures using collocated piezoelectric actuator and sensor.

The results of active control for the first three resonant modes are presented. The developed controller for each mode is tested individually and later combined in parallel so as to control any of the three modes of vibration. The performance of the combined controller is discussed and a comparison is made between the individual and the combined controllers.

## 2. BEAM MODEL USING ASSUMED MODES APPROACH

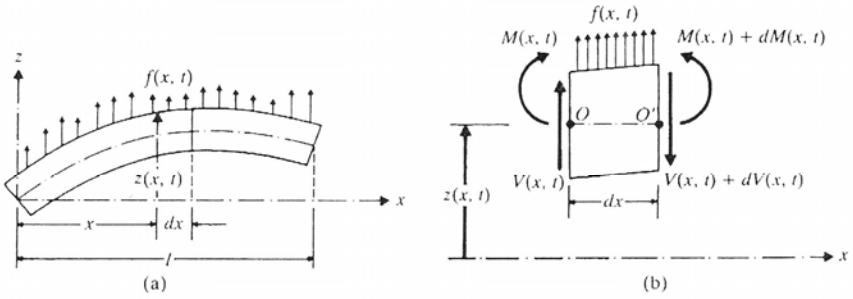


Fig. 1: Transverse vibration of beam [19].

Considering the equation of motion along the $z$-axis and the moment around $y$-axis at O leads to:

$$-(V+dV)+f(x,t)dx+V=\rho A(x)dx\frac{\partial^2 z(x,t)}{\partial t^2} \tag{1}$$

$$(M+dM)-M-(V+dV)dx+f(x,t)dx\frac{dx}{2}=0 \tag{2}$$

where $V$ = shear force, $M$ = bending moment, $f(x,t)$ = transverse force per unit length, $z(x,t)$ = transverse displacement, $\rho A(x)dx\frac{\partial^2 z(x,t)}{\partial t^2}$ = inertia force acting on beam, $\rho$ = mass density and $A(x)$ = cross sectional area.

Using the Euler-Bernoulli beam theory where $M(x,t) = EI(x)\frac{\partial^2 z}{\partial x^2}(x,t)$, Eq. (1) and Eq. (2) can be combined to yield Eq. (3)

$$EI(x)\frac{\partial^4 z}{\partial x^4}(x,t) + \rho A(x)\frac{\partial^2 z(x,t)}{\partial t^2} = f(x,t) \tag{3}$$

where $E$ = Young's modulus of the beam and $I(x)$ = area moment of inertia of the beam cross section about the neutral axis.

### 2.1 Model of beam with bonded piezoelectric patches

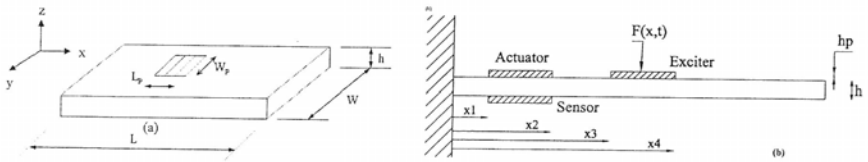


Fig. 2: (a) Piezoelectric patch on the beam with depicted dimension, and

(b) location of piezoelectric patches from fix end of the beam

Fig. 2 shows the position of attached piezoelectric patches on a cantilever beam. Dimension of the piezoelectric actuator is shown in the figure and a voltage $V_a(t)$ is applied to it.

Assuming the beam as a one dimensional system, Eq. (3) becomes:

$$EI(x)\frac{\partial^4 z}{\partial x^4}(x,t) + \rho A(x)\frac{\partial^2 z(x,t)}{\partial t^2} = \frac{\partial^2 M_a}{\partial x^2}(x,t) \tag{4}$$

where $M_a$ is the actuator induced bending moment and given by:

$$M_a = \overline{\mathrm{K}} V_a(t) \tag{5}$$

where $V_a(t)$ = voltage applied to piezoelectric actuator, $\overline{\mathrm{K}} = \frac{EI\kappa d_{31}}{h_p}$, $d_{31}$ = piezoelectric charge coefficient, $\kappa = \frac{12E_a h_p(h+h_p)}{2Eh^3 + E_a[(h+2h_p)^3 - h^3]}$, $E_a$ = piezoelectric elastic modulus, $h$ = plate thickness, and $h_p$ = piezoelectric thickness.

To incorporate the piezoelectric patch on the beam surface in the $x$ direction, Heaviside step function has been employed for the finite length of actuator. Using such Heaviside step function, Eq. (5) can be written as:

$$M_a = \overline{\mathrm{K}} V_a(t)\left[H(x-x_1) - H(x-x_2)\right] \tag{6}$$

where $x_1$ and $x_2$ are the distances of the piezoelectric actuator ends as given in Fig. 2(b).

Substituting beam's transverse displacement as $z(x,t) = \sum_{k=1}^{\infty} w_k(x) q_k(t)$ and Eq. (6) in Eq. (4) yields:

$$\frac{\partial^2 q_k(t)}{\partial t^2} + \omega_k^2 q_k(t) = \frac{\overline{\mathrm{K}} V_a(t)}{\rho A(x)}\left(w_k'(x_2) - w_k'(x_1)\right) \tag{7}$$

where $\omega_k$ = k-th mode natural frequency, $w'_k = dw_k / dx$, $w_k(x)$ is the k-th normal mode or characteristic function and $q_k(t)$ is the generalized coordinate in the k-th mode.

## 3. TRANSFER FUNCTIONS FOR SIMULATION STUDIES

Taking the Laplace transform of Eq. (7) gives:

$$q_k(s)\left[s^2 + \omega_k^2\right] = \frac{\overline{\mathrm{K}}\left(w_k'(x_2) - w_k'(x_1)\right)}{\rho A(x)} V_a(s) \tag{8}$$

Since, $Z_k(x,s) = w_k(x) q_k(s)$ Eq. (8) becomes:

$$Z_k(x,s) = \frac{w_k(x)\overline{\mathrm{K}}\left(w_k'(x_2) - w_k'(x_1)\right)}{\rho A(x)(s^2 + \omega_k^2)} V_a(s) \tag{9}$$

The transfer function that describes the elastic deflection of the entire beam due to an applied voltage to the actuator is given in Eq. (9). Incorporating proportional modal damping $\zeta_k$ to Eq. (9) gives [20]:

$$G_{voz}(x,s) = \frac{Z_k(x,s)}{V_a(s)} = \sum_{k=1}^{\infty} \frac{\left(\overline{\mathrm{K}}/\rho A(x)\right) w_k(x)\left(w_k'(x_2) - w_k'(x_1)\right)}{(s^2 + 2\zeta_k \omega_k s + \omega_k^2)} \tag{10}$$

### 3.1 Relationship between piezoelectric sensor and actuator voltages

Using Hooke's law for beam deflection in the $x$ direction, the strain experienced by the sensor patch is obtained as [21] :

$$\varepsilon_b(x,t) = -\left(\frac{h}{2} + h_p\right)\frac{\partial^2 z(x,t)}{\partial x^2} \tag{11}$$

The strain introduced in the beam will produce electric charge distribution per unit area in the piezoelectric sensor due to the piezoelectric effect. The electric charge distribution is given by

$q(x,t) = \frac{k_{31}^2}{g_{31}} \varepsilon_b$ where $k_{31}$ is the electromechanical coupling constant and $g_{31}$ is the piezoelectric stress constant. The total charge accumulated on the sensing layer can be found by integrating $q(x,t)$ over the entire surface area of the piezoelectric sensor, that is,

$$Q(t) = \int_{x_1}^{x_2} w_p q(x,t) dx = -w_p \left( \frac{h}{2} + h_a \right) \frac{k_{31}^2}{g_{31}} \frac{\partial z(x,t)}{\partial x} \Bigg|_{x_1}^{x_2} \tag{12}$$

where $w_p$ = width of the piezoelectric patch as shown in Fig. 2(a). Since charged piezoelectric patches can be considered as a parallel plate capacitor, the voltage across the layer is given by

$$V_s(t) = \frac{Q(t)}{C_p(x_2 - x_1)} = C_s \frac{\partial z(x,t)}{\partial x} \Bigg|_{x_1}^{x_2} \tag{13}$$

where $C_p$ is the patch capacitance, $x_2$-$x_1$ is the length of piezoelectric sensor and $C_s$ is expressed as

$$C_s = -w_a \left( \frac{h}{2} + h_a \right) \frac{k_{31}^2}{C_p g_{31}(x_2 - x_1)} \tag{14}$$

Combining Eq. (9), Eq. (13) and Eq. (14) yields

$$G_{vavs}(s) = \frac{V_s(s)}{V_a(s)} = \frac{C_s \overline{\mathrm{K}}}{\rho A(x)} \sum_{k=1}^{\infty} \frac{(w_k'(x_2) - w_k'(x_1))^2}{(s^2 + 2\zeta_k \omega_k s + \omega_k^2)} \tag{15}$$

### 3.2 Relationship between piezoelectric exciter voltage, sensor voltage and beam deflection.

Figure 2(b), shows the location of the piezoelectric exciter on the beam, where the applied force $F(x,t)$, which depends on the applied voltage $V_e(t)$ is used to excite the piezoelectric patch. The sensor voltage output for applied exciter voltage can be derived from Eq. (8) and is given by

$$V_s(s) = C_s \sum_{k=1}^{\infty} \frac{\overline{\mathrm{K}}(w_k'(x_4) - w_k'(x_3))(w_k'(x_2) - w_k'(x_1))}{\rho A(x)(s^2 + 2\zeta_k \omega_k + \omega_k^2)} V_e(s) \tag{16}$$

where $x_4$ and $x_3$ are the piezoelectric exciter ends from fix end of the cantilever beam as shown in Fig. 2(b). Eq. (16) subsequently gives

$$G_{vevs}(s) = \frac{V_s(s)}{V_e(s)} = C_s \sum_{k=1}^{\infty} \frac{\overline{\mathrm{K}}(w_k'(x_4) - w_k'(x_3))(w_k'(x_2) - w_k'(x_1))}{\rho A(x)(s^2 + 2\zeta_k \omega_k + \omega_k^2)} \tag{17}$$

$$G_{vez}(s) = \frac{Z(x,s)}{V_e(s)} = \sum_{k=1}^{\infty} \frac{\overline{\mathrm{K}} w(x)(w_k(x_4) - w_k'(x_3))}{\rho A(x)(s^2 + 2\zeta_k \omega_k + \omega_k^2)} \tag{18}$$

## 4. CONTROLLER DESIGN AND SIMULATION RESULTS

The above mathematical models lead to the block diagrams of Fig. 4 and Fig. 5 for the active control system. Here, an extra transfer function $G_{zvs}(s)$ as shown in Fig. 5, is introduced to transfer tip displacement to piezoelectric sensor voltage output since the reference input $V_i(s)$ is in voltage. Here $C(s)$ denotes the controller transfer function.

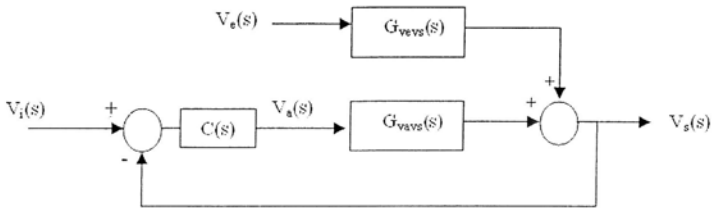


Fig. 3: Block diagram with feedback control for piezoelectric Sensor output ($V_s(s)$)

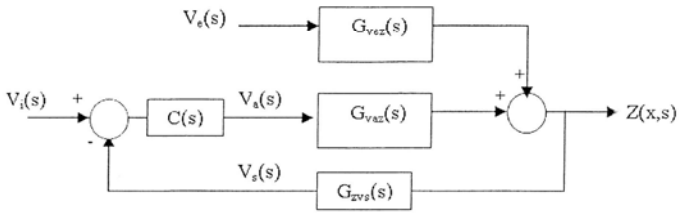


Fig. 4: Block diagram with feedback control for beam deflection (Z(x,s))

The block diagram reduction of Fig. 3 is given in Eq. (18), while that of Fig. 4, considering $G_{vavs}(s) = G_{vaz}(s)G_{zvs}$, leads to Eq. (19).

$$V_s(s) = \frac{G_{vevs}(s)V_e(s)}{1 + C(s)G_{vavs}(s)} + \frac{C(s)G_{vavs}(s)V_i(s)}{1 + C(s)G_{vavs}(s)} \tag{18}$$

$$Z(x,s) = \frac{G_{vez}(s)V_e(s)}{1 + C(s)G_{vavs}(s)} + \frac{C(s)G_{vaz}(s)V_i(x,s)}{1 + C(s)G_{vavs}(s)} \tag{19}$$

It is desired to have $V_i(s)$ equal to zero and the role of the controller is only to eliminate the effects of the disturbance force $F(x,t)$. Since a piezoelectric actuator is used as an exciter, the input force is controlled by its voltage $V_e(s)$.

### 4.1 Controller design

The choice of the controller is based on the need to have a high loop gain in either Eq. (18) or Eq. (19) in order to attenuate or eliminate the undesirable vibration modes. One possible approach, which has been adopted in this research work, is to use 'compensated inverse PID' (CIPID) controller of the form

$$C_k(s) = \sum_{k=1}^{3} \frac{s\left(\frac{1}{K_D}\right)\left(s + \frac{K_P}{K_D}\right)_k}{s^2 + \left(\frac{K_P}{K_D}\right)_k s + \left(\frac{K_I}{K_D}\right)_k} \tag{20}$$

where $K_P$, $K_I$ and $K_D$ are the gains of the PID which are tuned to damp k-th mode, where $\omega_k$ is the resonant frequency for k-th mode, that is:

$$\left(\frac{K_I}{K_D}\right)_k = \omega_k^2 \tag{21}$$

$$\left(\frac{K_P}{K_D}\right)_k = 2\zeta_k \omega_k \tag{22}$$

The subscript '$k$' in Eq. (20) stands for number of modes. Consequently, the CIPID behaves like a filter which can lead to the attenuation of undesirable vibration modes as the gains of the PID are carefully tuned.

The controller is designed to attenuate the first three modes of vibration. Using the superposition, the CIPID controller can be further arranged to control the first three modes as given in Eq. (20). The controller for each mode will be arranged in parallel. Basically the CIPID is used to damp the resonant peaks by placing zeros at each resonant frequency. Changing $K_P$ in the above equation will change the controller's damping factor for each mode and hence control the resonant peak. However higher damping factor does not mean that the peak will be always reduced. Hence an optimal value of $K_P$ is required for each mode. Fig. 5 shows the controller and beam with bonded piezoelectric patches. A digital low pass filter (not shown in Fig. 5) is applied to the sensor output to remove any interference signal or noise.

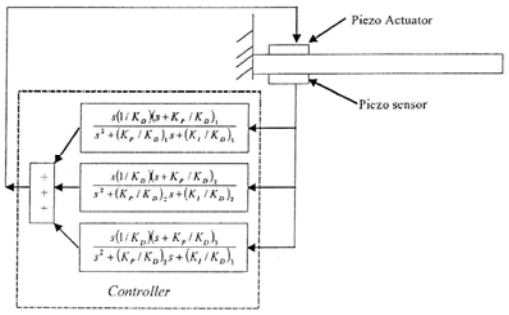


Fig. 5: Controller and beam with bonded piezoelectric patches.

### 4.2 Simulation results

The ability of the above controller in damping the resonant modes is investigated here. Different values of $K_P$, $K_I$ and $K_D$ are taken to study their effects on the resonant modes. An initial simulation is carried out for the individual mode. The individual controllers are then combined to damp all the three modes. In order to get more realistic simulation results, the damping factors and modes frequencies used for simulations in Eq. (10), (14) – (17) are determined experimentally for the beam used in this work and are given in Table 1.

Table 1: Experimental modal frequencies and damping ratios

| Modes | Frequency | $\zeta$ (damping ratio) |
|---|---|---|
| 1 | 11.14 | 0.02027 |
| 2 | 66.74 | 0.01021 |
| 3 | 186.64 | 0.00520 |

In this simulation studies, the value of $K_D$ is chosen to be 1, $K_I$ is taken from Eq. (21) and $K_P$ is adjusted by taking different values of $\zeta_c$ in Eq. (22). The simulation is carried out by changing the value of $K_P$ which correspondingly varies the damping ratio of the controller. The optimal values of $K_P$ can then be obtained. The results obtained for resonant peak reductions for $V_s$ are summarized in Table 2 which shows that the maximum reduction for the first mode at $\zeta_c = 0.5$ or $K_P = 11.141$. Smaller values of $\zeta_c$ may cause undesirable shift of the resonant frequency and introduce new peaks at the neighborhood of the actual frequency. For the second mode, greater reduction is achieved for $\zeta_c$=0.01. However, this value tends to introduce new peak on the left side of the resonant frequency, hence the most suitable value of $K_P$ is 2.2282. For similar reason, $K_P$ = 11.141 is selected to control the third mode.

Table 2: Simulation results for peak reductions (dB) for the first three modes

| $\zeta_k$ | $K_p$ | First Mode | Second Mode | Third Mode |
|---|---|---|---|---|
| 10 | 222.82 | 3.33 | 0.4 | 0.1 |
| 5 | 111.41 | 5.6 | 1.9 | 0.7 |
| 1 | 22.282 | 14.61 | 3.4 | 1.3 |
| 0.5 | 11.141 | **18.676** | 5 | **2.9** |
| 0.1 | 2.2282 | 15.121 | **11.46** | 11.5 |
| 0.01 | 0.2228 | 14.05 | 18.38 | -22.1 |

## 5. EXPERIMENTAL SETUP AND DATA ACQUISITION SYSTEM

An aluminum beam is used to carry out the experiment and the setup is shown in Fig. 6 and Fig. 7. The properties of the beam are given in Table 3. Three ACX piezoelectric patches are used in this research. Two unimorph patches model QP10W are collocated and used as sensor and actuator. One bimorph patch model QP25N is used as an exciter. Their properties are given in Table 4.

Table 3: Properties of the beam used for this work

| Parameter | Value | Unit |
|---|---|---|
| Length, L | 0.5 | m |
| Width, w | 0.04 | m |
| Thickness, h | 0.003 | m |
| Modulus of Young, E | $6.9 \times 10^{10}$ | $N / m^2$ |
| Area Moment of Inertia, I | $9 \times 10^{-11}$ | $m^4$ |
| Density, ρ | 2700 | $kg / m^3$ |
| Area, A | $1.2 \times 10^{-4}$ | $m^2$ |

The piezoelectric exciter is placed at the middle of the beam. However the piezoelectric actuator and sensor are collocated near the fixed end of the beam. The collocated sensor-actuator has minimum phase due to pole-zero interlacing [24, 25]. To obtain the highest damping factor, the piezoelectric patch is bonded on the structure in the area of highest strain energy. It is as been reported in [3, 26] that the highest strain energy for first three modes is at clamped boundary of the cantilever beam. Reference [26] showed that analytical equation can be used accurately to predict the optimum position of the piezoelectric patches. Hence, the piezoelectric sensor and actuator are attached at about 15 mm from the clamped end of the beam.

Two linear power amplifiers, having a gain up to 20 and an output voltage of ±200V are used in this experiment. A Keyence laser displacement sensor model LK-081 is used to measure the beam tip displacement. National Instruments (NI) data acquisition card model PCI-MIO-16XE-10 is used to acquire analog signal from the piezoelectric sensor and send the control signal to the piezoelectric actuator. A four channel HP-Dynamic signal analyzer (HP-DSA) model HP-35670A, is used to obtain beam resonant frequencies and respective damping ratios. Controlled and uncontrolled responses of the beam are measured and analyzed using the DSA.

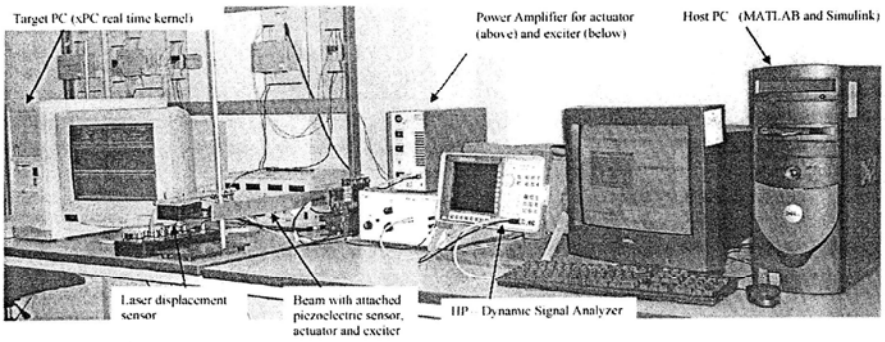


Fig. 6: The experimental setup for active vibration control.

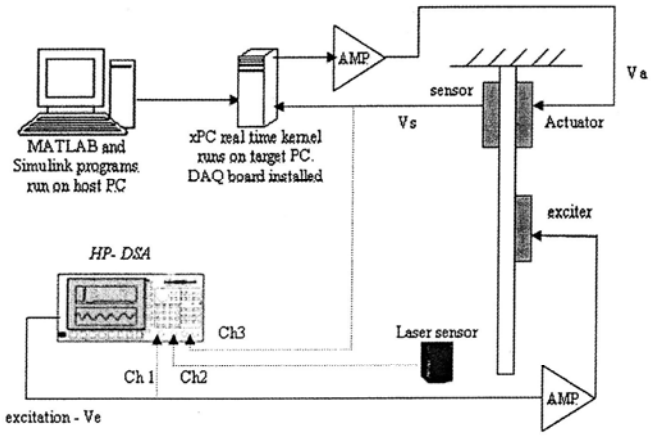


Fig. 7: Schematic diagram for the experimental setup.

Table 4: Properties of Piezoelectric Patches.

| Parameter | Units | QP 10 W (sensor/actuator) | QP 25 N (Exciter) |
|---|---|---|---|
| Length, $L_p$ | mm | 45.974 | 45.974 |
| Width, $w_p$ | mm | 33.274 | 20.574 |
| Height, $h_p$ | mm | 0.254 | 0.127 |
| Capacitance | μF | 0.1 | 0.2 |
| Coupling Coefficient, $k_{31}$ | | 0.3 | 0.4 |
| Elastic Modulus, $E_{11}$ | Pa | $6.9 \times 10^{10}$ | $6.3 \times 10^{10}$ |
| Elastic Modulus, $E_{31}$ | Pa | $5.5 \times 10^{10}$ | $5 \times 10^{10}$ |
| Charge Coefficient, $d_{31}$ | m / V | $-179 \times 10^{-12}$ | $-285 \times 10^{-12}$ |

Real-time implementation is carried out using xPC Target toolbox in MATLAB. This is a high-performance, host-target prototyping environment that enables the connection of Simulink models to physical systems and execute them in real-time on PC-compatible hardware [27]. xPC target enables the user to add I/O blocks to Simulink models, automatically generate code with Real-time Workshop, and download the code to a second PC running the xPC Target real-time kernel.

The HP-DSA is used to obtain transfer functions under controlled and uncontrolled condition. Signal from Ch2 divided by Ch1 gives transfer function for beam tip displacement to input excitation signal ($G_{vez}$) and signal Ch3 divided by Ch1 resulted in the transfer function, ($G_{vevs}$) for the piezoelectric-sensor arrangement.

# 6. EXPERIMENTAL RESULTS

## 6.1 Performance of the first mode controller

The beam is excited at its first resonant frequency which is 11.141 Hz to verify the performance of the controller in damping this mode. Fig. 8(a) and Fig. 8(b) show the reduction of gains $G_{vevs}$ and $G_{vez}$ respectively under controlled and uncontrolled conditions.

Figure 9 shows the reduction in peak-peak beam tip displacement upon switching on the controller. The first mode controller's performance is summarized in Table 5. Reduction of 17 dB or 92% is achieved for $G_{vevs}$ whereas a 22 dB is obtained for $G_{vez}$

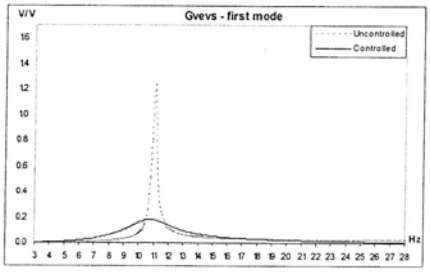


Fig. 8(a): Controlled and uncontrolled gain for $G_{vevs}$ for the first mode.

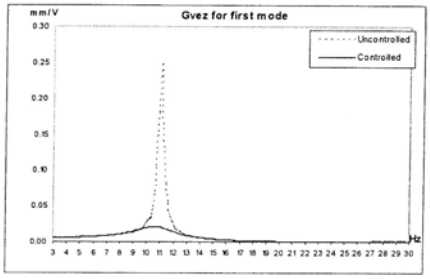


Fig. 8(b): Controlled and uncontrolled gain for $G_{vez}$ for the first mode.

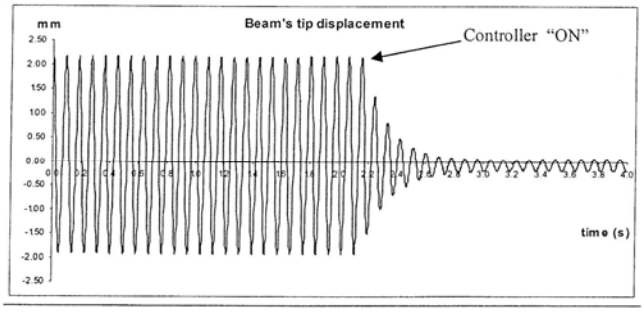


Fig. 9: Peak-peak displacement reduction at the beam's tip for the first mode.

Table 5: Performance of the first mode controller

| | $G_{vevs}$ *(V/V)* | $V_s$ *(volt)* | $G_{vez}$ *(mm/V)* | z *(mm)* |
|---|---|---|---|---|
| Uncontrolled | 1.2496 | 7.472 | 0.24980 | 2.562 |
| Controlled | 0.1765 | 0.878 | 0.01987 | 0.678 |
| Reduction | 1.0731 | 6.594 | 0.22993 | 1.884 |
| Reduction (dB) | **17.00** | **18.60** | **22.00** | **11.55** |
| Reduction ( % ) | **92.05** | **73.54** | **85.88** | **88.25** |

### 6.2 Performance of the second mode controller

The beam is excited at 66.744 Hz to produce second resonant mode. The controller's ability to damp the second mode is demonstrated in Fig. 10(a) and 10(b). Fig. 10(a) shows the reduction in gain for $G_{vevs}$ while Fig. 10(b) depicts that for $G_{vez}$. The percentage of reductions for both $G_{vevs}$ and $G_{vez}$ is summarized in Table 6.

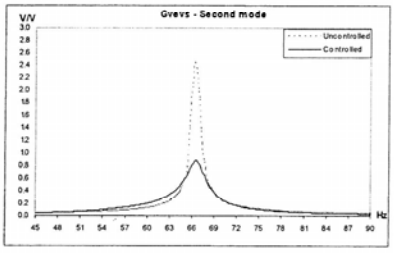


Fig. 10(a): Controlled and uncontrolled gain for $G_{vevs}$ for the second mode.

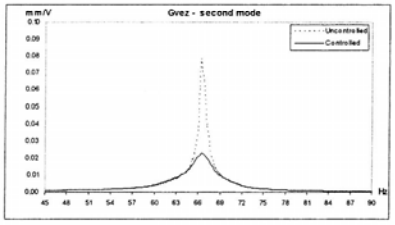


Fig. 10(b): Controlled and uncontrolled gain for $G_{vez}$ for the second mode.

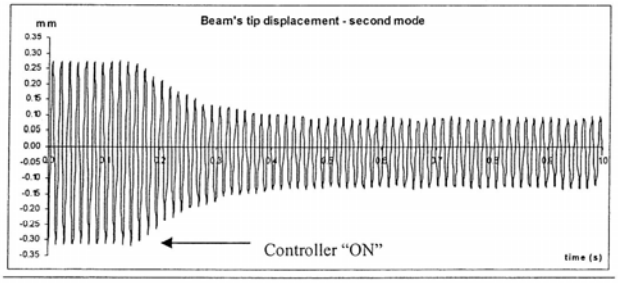


Fig. 11: Peak-peak displacement reduction at the beam's tip for the second mode.

Table 6: Performance of the second mode controller

| | $G_{vevs}$*(V/V)* | $V_s$*(volt)* | $G_{vez}$ *(mm/V)* | z *(mm)* |
|---|---|---|---|---|
| Uncontrolled | 2.4594 | 9.9517 | 0.07837 | 0.275 |
| Controlled | 0.8817 | 4.1592 | 0.02266 | 0.08177 |
| Reduction | 1.5777 | 5.7925 | 0.05571 | 0.19323 |
| Reduction (dB) | **8.910** | **7.58** | **10.78** | **10.53** |
| Reduction (%) | **64.15** | **58.21** | **71.09** | **70.27** |

### 6.3 Performance of the third mode controller

The beam is excited at its third resonant mode which is 186.6 Hz to evaluate the performance of third mode controller. The peak reduction for third mode is shown in Fig. 12 and summarized in Table 7. Due to hardware limitations, plots similar to Fig. 9 and Fig.12 could not be obtained for the third mode.

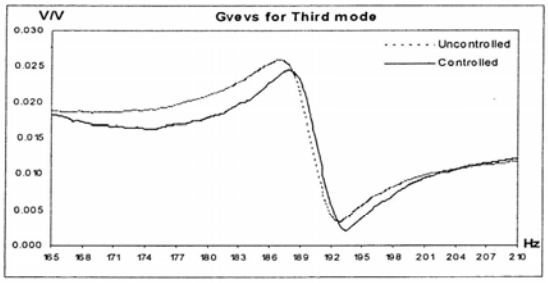


Fig. 12: Controlled and uncontrolled gain for $G_{vevs}$ for the third mode

Table 7: Performance of the third mode controller

| | $G_{vevs}$ *(V/V)* | $V_s$ *(volt)* |
|---|---|---|
| Uncontrolled | 0.02583 | 0.0921 |
| Controlled | 0.02374 | 0.0695 |
| Reduction | 0.00209 | 0.0226 |
| Reduction (dB) | **0.73287** | **2.4455** |
| Reduction (%) | **8.10** | **24.54** |

### 6.4 Performance of the combined controller

The individual mode controllers are combined in parallel to damp the vibration and the performance of this controller is discussed in this section. The beam is excited with sweep sine signal over the frequency range of 3 to 203 Hz, which comprises the first three resonant mode frequencies. The controlled and uncontrolled transfer function $G_{vez}$ and $G_{vevs}$ are shown in Fig. 13 and Fig. 14, respectively.

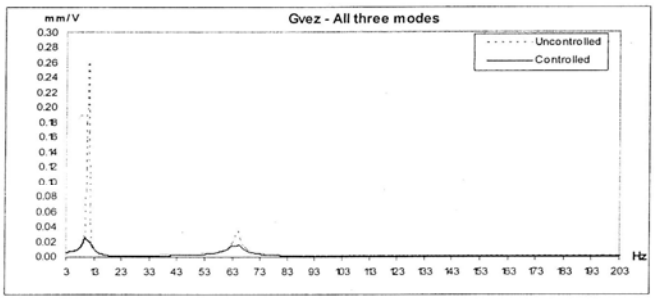


Fig. 13: Controlled and uncontrolled gain for $G_{vez}$ for the first three modes.

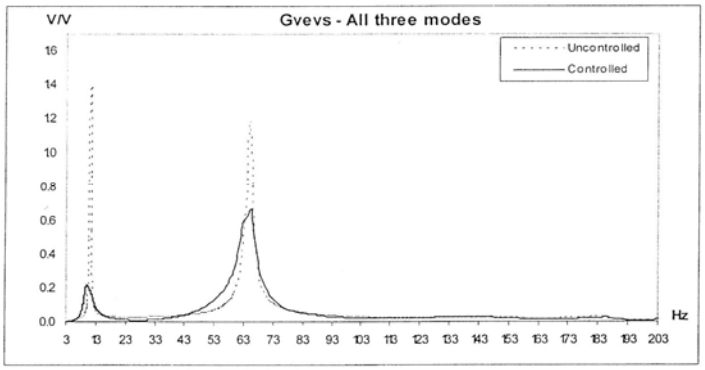


Fig. 14: Controlled and uncontrolled gain for $G_{vevs}$ for the first three modes.

The summary of peak reduction for the combined controller is given in Table 8. The third mode for $G_{vez}$ is not visible due to negligible gain. Table 9 shows the reduction in dB for first, second and third modes due to the application of individual and combined controllers to the beam.

Table 8: Performance of the combined controller.

| | $G_{vez}$ *(mm/V)* | | | $G_{vevs}$ *(V/V)* | | |
|---|---|---|---|---|---|---|
| Mode | 1st | 2nd | 3rd | 1st | 2nd | 3rd |
| Uncontrolled | 0.2584 | 0.0348 | - | 1.3879 | 1.1888 | 0.0294 |
| Controlled | 0.0191 | 0.0148 | - | 0.1945 | 0.5417 | 0.0280 |
| Reduction | 0.2394 | 0.02 | - | 1.1934 | 0.6471 | 0.0014 |
| Reduction (dB) | **22.65** | **7.41** | - | **17.07** | **6.8270** | **0.4240** |
| Reduction ( % ) | **92.63** | **57.41** | - | **86.00** | **54.43** | **4.76** |

Table 9: Reduction for the individual and combined controller.

| | Individual controller | | Combined controller | |
|---|---|---|---|---|
| mode | $G_{vcz}$ | $G_{vevs}$ | $G_{vez}$ | $G_{vevs}$ |
| 1st | 22.00 | 17.00 | 22.65 | 17.07 |
| 2nd | 10.78 | 8.91 | 7.41 | 6.827 |
| 3rd | - | 0.73 | - | 0.424 |

## 7. CONCLUSION

This paper has discussed the use of piezoelectric materials to control vibration of a cantilever beam. A controller that is based on inverse compensated PID has been designed and used to achieve this objective. The results of the real-time implementation of the controller using xPC target are found to be very close to that of simulation studies which actually demonstrates the effectiveness of this technique. Three individual controllers have been developed and its performances in suppressing the first three resonant modes have been examined. Also, the effects of combining the individual controllers were evaluated. In general, the combined controller has shown a better performance for $G_{vez}$ for the first mode while it produces relatively poorer performance for the second mode as compared to the performance of the individual controller. However, for $G_{vevs}$, the individual controller has shown reasonably better performance than the combined controller for second and third modes. The drop in the performance for combined controller is likely due to the coupling effects and further research work on this aspect is under investigation.

## 8. ACKNOWLEDGEMENT

The authors would like to thank IIUM research centre for partially funding this project under a short term research fund.

## 9. REFERENCES

[1] N. W. Hagood and A. H. von Flotow, "Damping of Structural Vibrations with Piezoelectric Materials and Passive Electrical Network" ,Journal of Sound and Vibration, Vol. 146, Issue 2, pp. 243-268, 1991.

[2] S. Y. Wu, "Method for Multiple Mode Shunt Damping of Structural Vibration Using Single PZT Transducer", Proc. SPIE, Smart Structures and Intelligent System, Vol. 3327, pp. 159-168, 1998.

[3] J. J. Granier, J. Hundhausen, and G. E. Gaytan, "Passive Modal Damping with Piezoelectric Shunts", Proc. SPIE, The Int. Society for Optical Eng., Vol. 1, Issue 4753, pp. 583-589, 2002.

[4] G. Caruso, "A Critical Analysis of Electric Shunt Circuits Employed in Piezoelectric Passive Vibration Damping", Smart materials and structures, Vol. 10, pp. 1059–1068, 2001.

[5] H. R Pota, S O. Reza Moheimani and Matthew Smith, "Resonant Controller for Smart Structures", Smart Materials and Structures, Vol. 11, pp. 1-8, 2002

[6] A. Baz and S.Poh, "Experimental Implementation of the Modified Independent Modal Space Control Methods", Journal of Sound and Vibration, Vol. 139, Issue 1, pp. 133-149, 1990.

[7] J. H. Hollkamp and T. F Starchville, "A Self Tuning Piezoelectric Vibration Absorber", Journal of Intelligent materials and system structures, Vol. 5, pp. 559-566, 1994.

[8] S. P. Kahn and K.W. Wang, "Structural Vibration Control via Piezoelectric Materials with Active –Passive Hybrid Networks", ASME - IMECE DE-75, pp. 187–94, 1994.

[9] M. J. Brennan, S.J. Elliott and R.J. Pinnington, "Strategies for the Active Control of Flexural Vibration on a Beam", Journal of Sound and vibration, Vol. 186, Issue 4, pp. 657-688, 1995.

[10] C. R. Fuller and A. H. Flotow, "Active Control of Sound and Vibration", IEEE Control Systems, Vol. 15, pp. 9–19, 1995. 1995

[11] J. Y. Andrew and H. H. Colin, "Control of Flexural Vibration in Stiffened Structures Using Multiple Piezoceramic Actuator", Applied Acoustics, Vol. 49, Issue 1, pp. 17-48, 1996.

[12] M.R. Bai, and G.M. Lin, "The Development of a DSP-Based Active Small Amplitude Vibration Control system for Flexible Beams by Using the LQG Algorithms and Intelligent Materials", Journal of Sound and Vibration, Vol. 198, Issue 4, pp. 411-427, 1996.

[13] G.S. Lee, "System Identification and Control of Smart Structures Using Neural Network", Acta Astronautica, Vol. 38, Issues 4-8, pp. 269-276, 1996.

[14] K. Yamamoto, T. Yamamoto, H. Ohmori, and A. Sano, "Adaptive Feedforward Control Algorithms for Active Vibration Control of Tall Structures", IEEE International conference on control applications, pp. 736-742, 1997.

[15] P. Gardonio and S. J. Elliott, "A Comparison of Active Control Strategies for the Reduction of Structural Vibration Transmission", Proc. 4th International Conference on Motion and Vibration Control, Zurich. Vol. 2, 1998.

[16] A. Lara, Jr. J. C. Bruch, J. M. Sloss, I.S. Sadek and S. Adali, "Vibration Damping in Beams via Piezoelectric Actuation Using Optimal Boundary Control", International Journal of Solids and Structures, Vol. 37, Issue 44, pp. 6537-6554, 2000.

[17] G. L. C. M Abreu, and J. F. Ribeiro, "Active Control of Flexible Structures Using Adaptive Fuzzy Controllers and Piezoelectric Patches", IFSA World Congress and 20th NAFIPS International Conference, Vol. 3, pp. 1764-1769, 2001.

[18] R. A. Morgan and K. W. Wang, "An Active-Passive Piezoelectric Absorber for Structural Vibration Control Under Harmonic Excitations with Time –Varying Frequency, Part 1: Algorithm Development and Analysis", ASME Journal of Vibration and Acoustics, Vol. 124, Issue 1, pp. 77-83, 2002.

[19] S. R. Singiresuo, "Mechanical Vibrations", Addison Wesley, 1995.

[20] S. O. Reza Moheimani, "Experimental Verification of the Corrected Transfer Function of a Piezoelectric Laminate Beam", IEEE Transactions on Control Systems Technology, Vol. 8, Issue 4, pp. 660-666, 2000.

[21] C. R. Fuller, S. J. Elliott and P.A. Nelson, "Active Control of Vibration", Academic Press, 1996.

[22] R. L. Clark, "Accounting for Out-of-Bandwidth Modes in the Assumed Modes Approach: Implications on Collocated Output Feedback Control", Trans. ASME J. Dynamic System., Measurement, Contr., vol. 119, 1997

[23] S. O. Reza Moheimani and R. L. Clark, "Minimizing the Truncation Error in Assumed Modes Models of Structures", ASME Journal of Vibration and Acoustics, vol. 122, Issue 3, pp. 332-335, 2000.

[24] R. L. Clark, W. R. Saunders and P. P. G. Gibbs, "Adaptive Structures", John Wiley & Sons, 1998.

[25] M. McEver and D. J. Leo, "Autonomous Vibration Suppression Using On-Line Pole-Zero identification", ASME Journal of Sound and Acoustics, Vol. 123, Issue 4, pp. 487–495, 2001.

[26] H. H. Law, P. L. Rossiter, G. P. Simon, and L.L. Koss, "Characterization of Mechanical Vibration Damping by Piezoelectric Materials", Journal of Sound and Vibration, Vol. 197, Issue 4, pp. 489-513, 1996.

[27] "xPC Target Selecting Hardware Guide-Manual", MathWorks, 2001.